Dispersion analysis of multi-modal waves based on the Reassigned Cross-S-Transform

Kristel Meza-Fajardo

Dispersion analysis of multi-modal waves based on the Reassigned Cross-S-Transform

By

Kristel C. Meza Fajardo

Submitted to:

Soil Dynamics and Earthquake Engineering

Author Affiliation:

Seismic and Volcanic Risk Unit, Risk and Prevention Division, BRGM.

3, avenue Claude-Guillemin, BP 36009 - 45060 Orléans cedex 2 – FRANCE

Tel : +33 (0) 2 38 64 36 91

E-mail : k.mezafajardo@brgm.fr

Abstract

The quantitative description of the propagation of the energy components in a signal is a fundamental task in signal processing. The correct identification of the components is important because they carry information about the medium in which they propagate. In this article, I introduce the Reassigned Cross-S-Transform to estimate dispersion curves from time-varying signals, a technique based on function maximization principles and time-frequency cross-correlation. The RCST provides a sharpened and direct estimate of the dispersion curve for multi-modal propagating waves. Furthermore, the RCST can be used with signals that are not synchronized with the same initial time. I present examples studying the degradation effects on the slowness curves due to mode mixture and reflected waves. I illustrate the application of the RCST technique to artificially generated Ricker wavelets, and to real recordings of seismic waves generated by an active source. Finally, using 2D numerical simulations of wave propagating through an elastic layered medium, I solve a mode identification problem by combining the RCST with a previously proposed technique to extract Rayleigh waves from signals.

Keywords: *geometrical dispersion, time-frequency analysis, multi-modal dispersion*.

1. Introduction

Analysis of recorded signals is fundamental in the understanding of wave propagation phenomena. The Fourier analysis has been a classical technique in the field of signal processing, due to its robust mathematical foundation and ease of application [1]. The Fourier spectrum provides insight on the energy of the signal as a function of frequency, allowing the identification of its components. Spectral analysis has been the basis of quantitative analyses and modeling of wave propagation problems in many fields such as physics, applied mathematics, and chemistry. However, most signals related to physical processes are *non-stationary*, this is, their frequency content change with time, and simple Fourier analysis cannot address this change. That is why many efforts have been devoted in the last decades to develop Time-Frequency Representations (TFR), being the most popular the Short-Time Fourier Transform [2], the Continuous Wavelet Transform [3], the Stockwell Transform [4], and the Empirical Mode Decomposition [5]. However, according to the Heisenberg-Gabor uncertainty principle [2], most of the TFRs mentioned above are of limited time-frequency resolution, leading in some cases to misidentification of components and poor readability. One technique that has been proposed to improve the readability of TFRs consists of *reassigning* the TFR so that the energy is concentrated at the time-frequency coordinates where the energy itself attains its maxima. According to Meignen *et al*. [6], this approach was initiated in the late 1970s by Kodera [7], after which many reassigned TFRs have been proposed for both non-invertible and fully invertible distributions. A recent comprehensive review on the subject of reassigned TFRs is provided in [6].

Among the different TFRs, the Stockwell Transform (also known as the S-Transform) has distinguished itself in practical applications because (i) it preserves the absolute phase of the

original time-domain signal, (ii) it can be inverted without losing information. These advantages have been exploited in recent seismological investigations, where the S-Transform has been successfully implemented for the identification and extraction of surface waves (Rayleigh and Love) from strong ground motion recordings, by characterizing the polarization characteristics of the different wave-types in the time-frequency domain [8]. Furthermore, the phase velocity of the extracted Rayleigh and Love waves was estimated in the time-frequency domain also making use of the Stockwell Transform [9]. In a previous publication [10], Stockwell himself had suggested the use of the Cross-Stockwell-Transform (CST) to estimate phase velocity among two stations, because the product of the two S-Transforms gives directly the phase difference for each point of the time-frequency space. However, this method gives correct results inasmuch as the peaks of the two signals are "located" at the same times.

In this work, I extend the ideas of Stockwell regarding the estimation of phase velocity from recorded signals to implement a time-frequency analysis that permits the estimation of the phase velocities of the waves making use of the reassignment technique. Different reassignment approaches have been already proposed for the S-Transform in order to improve its resolution, such as the generalized S-Transform [11] and the Synchrosqueezed S-Transform [12], among others. In particular Pan *et al*. [13] performed time-frequency cross-correlation analysis of signals using the Synchrosqueezed S-Transform, which allows the visualization of the change with time (the evolution) of the cross-correlation between two signals. Furthermore, the generalized S-Transform has been implemented by Askari *et al*. [14] in a slant stack procedure to compute dispersion curves of Rayleigh waves in terms of group velocities. Although the reassignment technique I propose herein indeed improves the resolution of the S-Transform, its main objective is to provide a Cross-S-Transform *with energy concentrated at the time-shifts*

63 *between two signals*, which directly gives the relation between slowness and frequency, namely,
64 *the dispersion curve*. Since spreading of energy is one of the difficulties in identifying different
65 modes in dispersion analysis, especially when the modes are close to each other (in frequency)
66 (see for instance, Levshin and Panza [15]), a dispersion curve obtained from reassignment could
67 be useful to the misidentification problem. Furthermore, as I will show in the sequel, the
68 *Reassigned Cross-S-Transform* (RCST) is basically a mathematical maximization technique
69 applied to the S-Transform of the signals, and I make no assumptions regarding the physical
70 processes represented in the signals: no assumptions regarding either the type of waves or the
71 spatial-temporal distribution of the phase velocity. Thus, the technique can be applied to signals
72 related to any wave-propagation problem, provided that they are correctly sampled, as any other
73 signal processing technique requires.

74 In this article I consider a natural application of the reassignment technique, the dispersion
75 analysis of Rayleigh waves, since they are waves with strong dispersive characteristics.
76 Multimodal dispersion analysis of Rayleigh waves is a very common tool for in-situ, non-
77 destructive testing of different types of materials. In near-surface geophysics in particular, a
78 popular technique used in seismic surveys is the use of the dispersion curve of Rayleigh waves
79 propagating through the surface, to derive the shear wave velocity of the different soil layers at a
80 specific site [16]. The Rayleigh waves are recorded at an arrangement of sensors after they are
81 excited by a blast or by a sledgehammer. However, in the obtained seismic wave field different
82 types of waves are present (body, Love, reflected, scattered, noise), which can have a detrimental
83 impact on the estimation of the desired dispersion curve. Different wave types and different
84 modes of similar frequency arriving at neighboring times can interfere and degrade the accuracy
85 of the estimated velocities. Addressing these inaccuracies is still a problem of interest in near-

surface geophysics, as the correct determination and interpretation of the dispersion curve is a fundamental step in a successful surface-wave testing campaign [17] .

In the following sections, I first explain the basic concepts about the S-transform and about dispersion curves based on measurements of phase velocity. I then derive the mathematical formulation to reassign the S-transform of a signal, and extend the reassignment ideas to derive the Reassigned Cross-S-Transform (RCST). Later, I illustrate the applicability of the RCST with three experiments of artificial dispersive waves: one with a single wave train, a second one with two dispersive modes propagating in the same direction, and a third one with two modes propagating in opposite direction. I implement this last synthetic experiment in order to asses the effect of reflected waves on the RCST. I also analyse a set of real recordings, acquired to be analysed with the method of Multichannel Analysis of Surface Waves (MASW) [18], and compare the obtained dispersion curve with estimations from the more classical F-K Transform technique. Finally, I illustrate the advantages of using recordings of several components (horizontal and vertical) to identify and separate different modes of surface waves, and in turn, to improve the estimation of the dispersion curve. For this, I consider a seismic wave field generated through 2D numerical simulations with the Spectral Element Method, in a layered velocity structure where several Rayleigh wave modes propagate.

2. Dispersion analysis and the S-transform

Dispersion phenomena is observed when the phase velocity of a wave is frequency-dependent. In seismological processes dispersion is of two types: material dispersion due to viscoelastic attenuation, and geometric dispersion due to heterogeneity of the medium [19]. Regardless of the type of dispersion, a frequency-dependent phase velocity can be defined as follows:

$$v_p(f_n) = \frac{d}{t_p}, \quad t_p = t_p(f_n) \tag{1}$$

for each frequency f_n, where d is the propagation distance (the distance between the two nearby stations where the signals are observed/recorded). The parameter t_p (the time shift) is then the physical quantity that remains frequency-dependent. Phase velocity is a convenient mechanical parameter to describe a medium, because the time shift t_p is a quantity that can be simply and directly measured, without making any assumptions regarding the physical process. Alternatively, a dispersion curve can be expressed in terms of a frequency-dependent phase slowness:

$$s_p(f_n) = \frac{t_p(f_n)}{d} \tag{2}$$

In this work, I will then focus on estimating t_p for wave trains present in two signals recorded at nearby stations separated by an interstation distance d. In addition, I express the dispersion curves in terms of the phase slowness, because of its simple proportionality [Eq. (2)] with the time shift. The time shift is in turn related to the phase shift φ_s by the simple equation:

$$t_p(f_n) = \frac{\varphi_s}{2\pi f_n}, \quad \varphi_s = \varphi_s(f_n) \tag{3}$$

where clearly the phase shift is also a frequency-dependent quantity. A classical wave to estimate φ_s for a propagating monochromatic wave is to find the peaks of the amplitude of the two signals and then take the corresponding phase difference. When the signals are composed of several overlapping wave trains, finding such peaks with time-domain processing techniques can be a problematic task. Here is when a TFR of the signals becomes a more appropriate tool of analysis, since the TFRs provide the evolution of the different frequency components of the signals. The TFR I adopted for this study is the Stockwell-Transform, which is defined as follows [4]:

$$S(t, f_n) = \int_{-\infty}^{\infty} u(\tau) \frac{|f_n|}{\sqrt{2\pi}} \exp\left[-\frac{(t-\tau)^2 {f_n}^2}{2}\right] \exp(-2\pi i f_n \tau) d\tau \quad (4)$$

where of $u(t)$ is the signal to be transformed. At each frequency f_n the S-transform provides a time function called a "voice", which results from filtering the signal so as to isolate the time history of only the f_n component. Since each value of the S-transform is a complex number, it can also be expressed in polar form:

$$S(t, f_n) = A \exp(i\varphi), \quad A = A(t, f_n), \quad \varphi = \varphi(t, f_n) \quad (5)$$

where $A(t, f_n)$ is the amplitude of the complex number, φ is the phase, and $i = \sqrt{-1}$. Let us note that the phase φ provided by the S-transform is the same phase of the signal at the point (t, f_n) [4]. One straightforward way to compute the phase-shift between two voices is to identify the location (in time) of the amplitude maxima, and then extract the phase difference at those times. However, this method cannot be performed in an automatic manner if there are different wave trains present in the signal. For signals composed of single wave trains, the method of computing the phase difference using the Fourier Transforms of the signals [20] is much more economic, and as accurate. Stockwell [4] had proposed a method of computing the phase difference from the Cross-S-Transform of the two signals, which is defined as:

$$S_{12}(t, f_n) = S_1 \cdot \bar{S_2} \quad (6)$$

where S_1 and S_2 are the S-Transforms at stations 1 and 2, respectively, and $\bar{S_i}$ denotes the complex conjugate of S_i. Station 2 is the station at which the waves arrive later. Using the polar forms, the phase difference follows directly:

$$S_{12}(t, f_n) = A_1 \cdot A_2 \exp(i\varphi_1 - i\varphi_2) \quad (7)$$

However, for this method to give the correct phase difference, the peaks of the amplitude of the voices of the two S-Transforms should be located at the same time. Besides, if several wave trains are present in the signal, they need to be treated one at a time, after identification.

3. Reassignment of the S-transform

The idea of reassigning the S-transform consists in concentrating the energy of the TFR around the coordinates (t, f) where the energy itself reaches its maximum values. These coordinates are usually referred to as the time delay and the instantaneous frequency. The *time delay* is identified as the time of arrival of the peak of the envelope of an analytical signal. The *instantaneous frequency* is the frequency around which the spectral energy is concentrated at a specific time. These concepts are immediately applied to the peaks of the amplitude of the S-Transform, since each voice of the S-transform is equivalent to a band-pass filtered analytical signal of the original time function [10]. Therefore, the time delay t_d is identified by finding the arrival time of $\max_t A(t, f_n)$. Consequently, in the S-Transform domain the time delay is found at the instants when the derivative of the amplitude is zero:

$$\left.\frac{dA(t, f_n)}{dt}\right|_{t=t_d} = 0 \tag{8}$$

Note that the amplitude of a complex number is a positive function, thus there will be no "negative peaks". The problem of finding the time delay is then a maximization problem. The derivative in Eq. (8) can be approximated numerically, however here I prefer to derive analytic expressions for it. I start by recalling the polar form of the S-Transform [Eq. (5)] and applying natural logarithm:

$$\ln[S(t, f_n)] = \ln[A(t, f_n)] + i\varphi(t, f_n) \tag{9}$$

161 Taking the *time* derivative of the logarithmic expression, the following expression is obtained:

$$\frac{1}{S(t,f_n)}\frac{dS(t,f_n)}{dt} = \frac{1}{A(t,f_n)}\frac{dA(t,f_n)}{dt} + i\frac{d\varphi(t,f_n)}{dt} \tag{10}$$

162 In view of the fact that $A(t,f_n)$ & $\varphi(t,f_n)$ are *real* quantities, it is true that:

$$\frac{1}{A(t,f_n)}\frac{dA(t,f_n)}{dt} \;=\; \mathcal{R}e\left\{\frac{1}{S(t,f_n)}\frac{dS(t,f_n)}{dt}\right\} \tag{11}$$

163 where $\mathcal{R}e\{\cdot\}$ denotes the real part of its argument. Starting from the definition of S-Transform

164 given in Eq. (4), it is straightforward to derive an expression for the derivative $dS(t,f_n)/dt$:

$$\begin{aligned}\frac{dS(t,f_n)}{dt} &= -\int_{-\infty}^{\infty} u(\tau)\frac{|f_n|}{\sqrt{2\pi}}\exp\left[-\frac{(t-\tau)^2 {f_n}^2}{2}\right]\exp[-2\pi i f_n\tau]\,(t-\tau){f_n}^2 d\tau \\ &= -t{f_n}^2 S(t,f_n) + {f_n}^2 S_t(t,f_n)\end{aligned} \tag{12}$$

165 where $S_t(t,f_n)$ is the S-Transform of the product $t\cdot u(t)$:

$$S_t(t,f_n) = \int_{-\infty}^{\infty} \tau u(\tau)\frac{|f_n|}{\sqrt{2\pi}}\exp\left[-\frac{(t-\tau)^2 {f_n}^2}{2}\right]\exp[-2\pi i f_n\tau]\,d\tau \tag{13}$$

166 From re-arranging expression (12) above, I obtain the expression:

$$\frac{1}{S(t,f_n)}\frac{dS(t,f_n)}{dt} \;=\; {f_n}^2\left[\frac{S_t(t,f_n)}{S(t,f_n)} - t\right] \tag{14}$$

167 Using the latter result in Eq. (11) gives:

$$\frac{dA(t,f_n)}{dt} \;=\; {f_n}^2\left(\mathcal{R}e\left\{\frac{S_t(t,f_n)}{S(t,f_n)}\right\} - t\right)A(t,f_n) \tag{15}$$

168 Consequently, the analytical expression for the time delay is obtained:

$$\left.\frac{dA(t,f_n)}{dt}\right|_{t=t_d} = 0 \;\;\Rightarrow\;\; t_d(f_n) \stackrel{\text{def}}{=} \mathcal{R}e\left\{\frac{S_t(t_d,f_n)}{S(t_d,f_n)}\right\} \tag{16}$$

The time delay computed with Eq. (16) requires the computation of two transforms, the S-Transform of $u(t)$ and the S-transform of $t \cdot u(t)$. An analytical expression can be also derived for the *Instantaneous Frequency*, which may be defined as follows [10]:

$$IF(t) \quad \stackrel{\text{def}}{=} \quad \frac{1}{2\pi}\frac{\partial}{\partial t}\{2\pi f_n t + \varphi(t, f_n)\} \tag{17}$$

From Eq. (10) is evident that:

$$\frac{d\varphi(t, f_n)}{dt} \quad = \quad \mathcal{Im}\left\{\frac{1}{S(t, f_n)}\frac{dS(t, f_n)}{dt}\right\} \tag{18}$$

where $\mathcal{Im}\{\cdot\}$ denotes the imaginary part of its argument. Using Eq. (14) the result for the Generalized Instantaneous Frequency is obtained:

$$GIF(t, f_n) = f_n + \left(\frac{f_n^2}{2\pi}\right)\mathcal{Im}\left\{\frac{S_t(t_d, f_n)}{S(t_d, f_n)}\right\} \tag{19}$$

Similarly, a Generalized time-frequency distribution of the time delay can be defined as:

$$T_d(t, f_n) \stackrel{\text{def}}{=} \mathcal{Re}\left\{\frac{S_t(t, f_n)}{S(t, f_n)}\right\} \tag{20}$$

which is then used to reassign the S-Transform through the sifting effect of convolving $S(t, f_n)$ with the Delta-Dirac function:

$$S_R(T_d, f_n) = \int_{-\infty}^{\infty} S(\tau, f_n)\, \delta(T_d - \tau) d\tau \tag{21}$$

What the reassignment means is that the S-transform is now evaluated at the coordinates (T_d, f_n), the energy is concentrated in the neighboring of the time-delay t_d, and thus the localization of energy is more precise. Now, in order to obtain a dispersion curve I am not interested in concentrating the energy around t_d, the time delay at each station, but around t_p, *the time shift*

between the two stations [given in Eq. (2)]. This will provide the variation of t_p with frequency, without the need of finding any maxima, and all waves present in the signal are automatically considered. Thus, instead of reassigning each individual S-transform, I want to *reassign the Cross-S-Transform* [as given in Eq. (6)].

4. Reassignment of the Cross-S-Transform

Following the ideas of the reassigned S-transform presented in the previous section, I want to reassign the Cross-S-Transform (CST) on a time-frequency distribution of the time-shift, that I denote here by T_p, in the following manner

$$S_{RC}(T_p, f_n) = \int_{-\infty}^{\infty} S_C(\tau, f_n)\, \delta(T_p - \tau) d\tau \tag{22}$$

and using a redefined Cross-S-Transform:

$$S_C(t, f_n) = S_1 \cdot \bar{S}_{2s} \tag{23}$$

where now S_1 is multiplied by the shifted S-Transform of station 2, S_{2s}. More precisely, S_{2s} is the result of shifting each voice of S_2, so that the amplitude peaks of S_1 and S_{2s} are located at the same times. Because the voices are functions of time, the delay between two voices is simply obtained by applying time-domain cross-correlation to each pair of voices:

$$t_l(f_n) = \underset{t}{\operatorname{argmax}} \int_{-\infty}^{\infty} S_1(\tau, f_n) S_2(\tau + t, f_n) d\tau \tag{24}$$

And then each voice $S_2(\tau, f_n)$ is shifted t_l seconds to obtain $S_{2s}(\tau, f_n)$. The effect of a shift in time of the S-Transform becomes evident when expressing the S-Transform as the inverse Fourier Transform of a convolution [10]:

$$S(\tau, f_n) = \int_{-\infty}^{\infty} U(\alpha + f_n) \frac{|f_n|}{\sqrt{2\pi}} \exp\left[-\frac{2\pi^2\alpha^2}{{f_n}^2}\right] \exp(2\pi i\alpha\tau) d\alpha \tag{25}$$

198 Letting $\tau = t - t_l(f_n)$

$$\begin{aligned} S(t - t_l, f_n) &= \exp(-2\pi i\alpha t_l) \int_{-\infty}^{\infty} U(\alpha + f_n) \frac{|f_n|}{\sqrt{2\pi}} \exp\left[-\frac{2\pi^2\alpha^2}{{f_n}^2}\right] \exp(2\pi i\alpha t) d\alpha \\ &= \exp(-2\pi i\alpha t_l) S(t, f_n) \end{aligned} \tag{26}$$

199 Therefore, $S_{2s}(t, f_n)$ can be obtained by simply multiplying each voice of $S_2(t, f_n)$ by the
200 corresponding complex exponential $\exp(2\pi i\alpha t_l)$, where $t_l = t_l(f_n)$. At this point I would like to
201 remark that the shifted transform $S_{2s}(t, f_n)$ will be the same even if the signal at station 2 does
202 not have the same initial time at station 1. With different initial times the parameter $t_l(f_n)$ will be
203 different from the case of having the same initial time, but not the final result $S_{2s}(t, f_n)$. And
204 thus the technique I propose herein can be used to compute phase velocities even for data that is
205 not synchronized with the same initial time.

206 In what follows, I present how the expression for T_p can be derived, T_p being the Generalized
207 Time-Shift once the two S-Transforms have the peaks at the same coordinates. I start by
208 recognizing the analogy between the time delay and the time shift: the time delay gives the
209 localization in time of each amplitude peak of the S-transform, and the time shift is associated to
210 peaks of the CST. In both cases a maximization is made, that is, time values are found such that
211 derivatives are zero. Since the CST is also a complex number, it can be expressed in polar form:

$$S_C(t, f_n) = A_C \exp(i\varphi_d), \qquad A_C = A_C(t, f_n), \qquad \varphi_d = \varphi_d(t, f_n) \tag{27}$$

212 where φ_d is the phase difference between S_1 and S_{2s}. From Eq. (23) I recall that the CST is the
213 product of two complex-valued functions, its derivative then is given by:

$$\frac{dS_C(t,f_n)}{dt} = S_1(t,f_n)\frac{d\bar{S}_{2s}(t,f_n)}{dt} + \frac{dS_1(t,f_n)}{dt}\bar{S}_{2s}(t,f_n) \quad (28)$$

214 Using Eq. (14) the following expressions are obtained:

$$S_1(t,f_n)\frac{d\bar{S}_{2s}(t,f_n)}{dt} = S_1(t,f_n)\left[-t{f_n}^2\bar{S}_{2s}(t,f_n) + {f_n}^2\bar{S}_{2st}(t,f_n)\right] \quad (29)$$

$$\frac{dS_1(t,f_n)}{dt}\bar{S}_{2s}(t,f_n) = \left[-t{f_n}^2 S_1(t,f_n) + {f_n}^2 S_{1t}(t,f_n)\right]\bar{S}_{2s}(t,f_n)$$

215 These results can then be substituted in Eq. (28):

$$\frac{dS_C(t,f_n)}{dt} = -2t{f_n}^2 S_C(t,f_n) + {f_n}^2[S_1(t,f_n)\bar{S}_{2st}(t,f_n) + S_{1t}(t,f_n)\bar{S}_{2s}(t,f_n)] \quad (30)$$

216 Thus the derivative of the CST can be found by evaluating four S-transforms. Now, different
217 from the case of the time delay, I will not focus here on finding a time when the derivative of an
218 amplitude is zero as in [Eq. (16)]. Here the goal is to find the phase shift *when the total*
219 *derivative of the CST is zero*. To show that this is the case I go back to Eq. (27) and take the
220 logarithm

$$\ln S_C(t,f_n) = \ln A_C(t,f_n) + i\varphi_d(t,f_n) \quad (31)$$

221 The derivative will then be:

$$\frac{1}{S_C(t,f_n)}\frac{dS_C(t,f_n)}{dt} = \frac{1}{A_C(t,f_n)}\frac{dA_C(t,f_n)}{dt} + i\frac{d\varphi_d(t,f_n)}{dt} \quad (32)$$

222 It is then clear that enforcing a zero total derivative implies not only that the derivative of the
223 amplitude of the CST at some time t_s is zero, but also that the derivative of its phase is zero at t_s.

$$\left.\frac{d\varphi_d(t,f_n)}{dt}\right|_{t=t_s} = 0 \quad (33)$$

The underlying assumption is then

$$\frac{d\varphi_1(t_s, f_n)}{dt} = \frac{d\varphi_2(t_s, f_n)}{dt} \tag{34}$$

To understand that this is the case, let me recall that the peaks of $S_1(t, f_n)$ and $S_{2s}(t, f_n)$ are located at the same (t, f) coordinates, which is equivalent to say that $S_1(t, f_n)$ and $S_{2s}(t, f_n)$ have *the same time delay* t_d and *the same instantaneous frequency*. Thus, from the definition of IF given in Eq. (17) it is evident that relation (34) must hold. Furthermore, if $t_s = t_d$, the derivatives of the amplitudes A_1 and A_2 are zero at t_s, and consequently, the derivative of A_c at t_s must be zero too. I now proceed to enforce a zero-derivative of the CST:

$$\begin{aligned}\frac{dS_C(t_s, f_n)}{dt} &= -2t_s {f_n}^2 S_C(t_s, f_n) + {f_n}^2[S_1(t_s, f_n)\bar{S}_{2st}(t_s, f_n) + S_{1t}(t_s, f_n)\bar{S}_{2s}(t_s, f_n)] \\ &= 0\end{aligned} \tag{35}$$

Solving for $S_C(t_s, f_n)$, the result is the following

$$2tS_C(t_s, f_n) = [S_1(t_s, f_n)\bar{S}_{2st}(t_s, f_n) + S_{1t}(t_s, f_n)\bar{S}_{2s}(t_s, f_n)] \tag{36}$$

Since $S_C(t_s, f_n) = A_C(t_s, f_n)\exp[i\varphi_d(t_s, f_n)]$ the latter expression becomes:

$$2tA_C(t_s, f_n)\exp[i\varphi_d(t_s, f_n)] = [S_1(t_s, f_n)\bar{S}_{2st}(t_s, f_n) + S_{1t}(t_s, f_n)\bar{S}_{2s}(t_s, f_n)] \tag{37}$$

Now taking the natural logarithm

$$\ln 2tA_C(t_s, f_n) + i\varphi_d(t_s, f_n) = \ln[S_1(t_s, f_n)\bar{S}_{2st}(t_s, f_n) + S_{1t}(t_s, f_n)\bar{S}_{2s}(t_s, f_n)] \tag{38}$$

Solving for φ_d I then obtain the phase shift under the maximization conditions:

$$\varphi_d(t_s, f_n) = \mathcal{Im}\{\ln[S_1(t_s, f_n)\bar{S}_{2st}(t_s, f_n) + S_{1t}(t_s, f_n)\bar{S}_{2s}(t_s, f_n)]\} \tag{39}$$

And from this results I defined a TFR which I call the Generalized Phase Shift:

$$\Phi_d(t, f_n) = \mathcal{Im}\,\{\ln[S_1(t, f_n)\bar{S}_{2st}(t, f_n) + S_{1t}(t, f_n)\bar{S}_{2s}(t, f_n)]\} \tag{40}$$

Finally, with substitution of this result in Eq. (3) I obtain a TFR for the time shift, that is, the *Generalized Time Shift*:

$$\mathrm{T}_p(t, f_n) = \frac{1}{2\pi f_n}\mathcal{Im}\,\{\ln[S_1(t, f_n)\bar{S}_{2st}(t, f_n) + S_{1t}(t, f_n)\bar{S}_{2s}(t, f_n)]\} \tag{41}$$

With this key result I can re-assign the Cross-S-Transform, using Eq. (22). In the next sections I illustrate how all these theoretical derivations can be used to obtain dispersion curves.

5. Example with one artificial dispersive wave train

In this example, I propagate a Ricker wavelet through different stations, imposing an artificial dispersion curve. The Ricker wavelet is given by the expression:

$$R(t) = A_R(2\beta - 1)\exp(-\beta), \qquad \beta = [\pi f_c(t - t_c)]^2 \tag{42}$$

where A_R is the amplitude and t_c is the time of its largest peak. The Ricker wavelet has a limited bandwidth with energy concentrated at its central frequency f_c. This limited bandwidth is one of the reasons why the Ricker wavelet is used in many seismological applications, since registered seismograms are usually composed of several wave trains of limited duration and limited frequency band. To propagate this wavelet with frequency-dependent phase velocity I adopt the following artificial dispersion curve:

$$V_p = 1.7\exp\left(-\frac{f}{15}\right) + 0.4 \quad \left(\frac{km}{s}\right) \tag{43}$$

In Figure 1 I plot this dispersion curve given in terms of phase velocity, and most importantly, in terms of the slowness. With this artificial slowness, I propagate the dispersive Ricker wavelet at 20 stations, with a uniform interstation distance Δx of 5 m (typical in geophysical measurements). For the Ricker wavelet I choose $A_R = 1$, $f_c = 30\ Hz$, and $t_c = 1/f_c$. In order to

have precise measurements of small time shifts, I select the time step Δt to be 1.43E-4 s. For each discrete frequency, I apply the time shift to the Ricker wavelet in the frequency domain via the Fourier Transform and convolution. Thus, the waveform at some station $j+1$ is obtained from the waveform at station j:

$$R_{j+1}(t) = F^{-1}\{F\{R_j(t)\} \cdot \exp(-2i\pi f s_p \Delta x)\} \tag{44}$$

where $s_p = s_p(f)$ is the slowness, and $F\{\cdot\}$ and $F^{-1}\{\cdot\}$ denote the Fourier Transform operator and its inverse, respectively. The obtained waveforms at the 20 stations corresponding to the slowness of Figure 1b are illustrated Figure 2, where the duration of the wave train with distance can be appreciated.

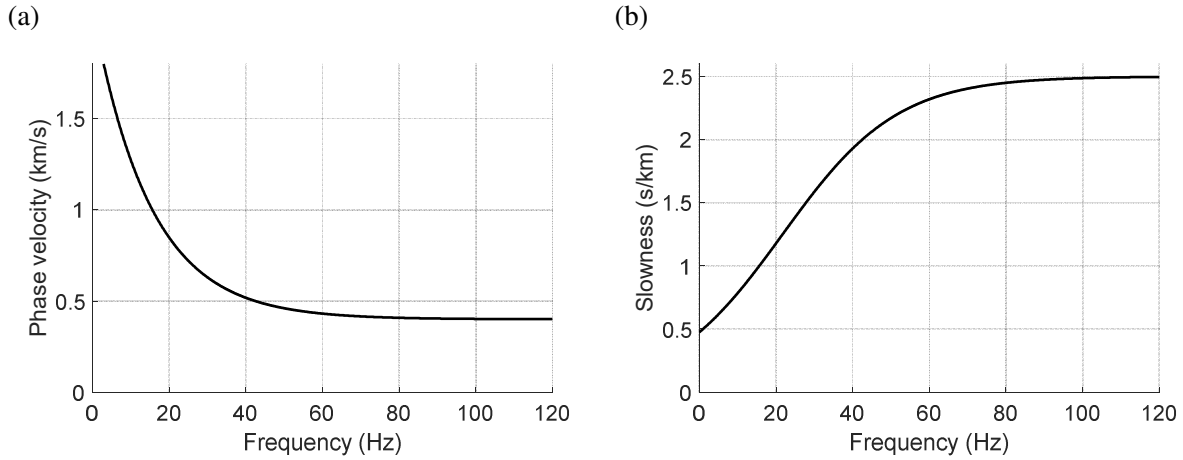

Figure 1. Artificial (a) phase velocity and (b) slowness for single dispersive Ricker wave train.

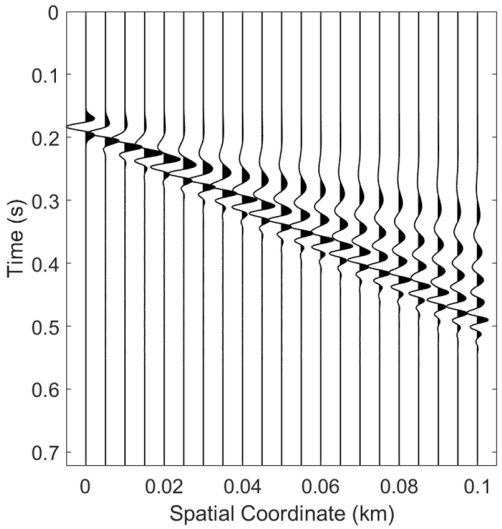

Figure 2. Waveforms at 20 stations for a single Ricker wavelet with artificial dispersion.

In order to further illustrate the dispersion effect, in Figure 3a and 3b I show the S-Transform of the signals at the first and last stations. The separation of the arrival times of the peaks of the amplitude of the S-Transform at the final station is evident, even though the components of the waveform are not separated, and at the final station it can be still considered that a single wave train is present in the signal. Although not a necessary step in the procedure, in Figures 3c and 3d I show the reassigned S-Transforms at the first and last stations using the time delay t_d, to illustrate the sharpening effect of reassignment. After reassignment the peaks of the S-transforms can be more precisely identified. With this artificial example I will recover the dispersion curve using the seismograms at the first and the final stations of the arrangement, because there is no wave interference or loss of energy in the propagated wave. In more realistic settings, interaction with other waves and geometrical and material attenuation would require the use pairs of stations that are as close as possible.

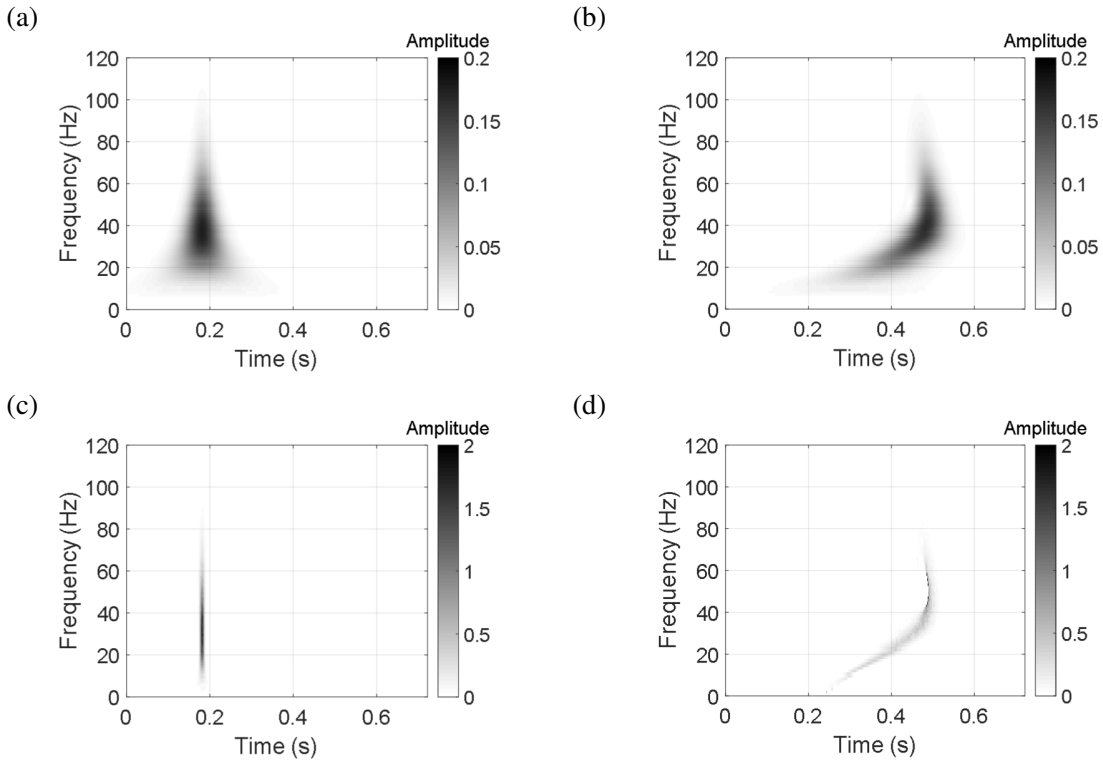

Figure 3. Amplitude of S-transforms of dispersed Ricker wavelet. (a) S-transforms at first station, (b) S-transforms at final station, (c) Reassigned S-transforms at first station (d) Reassigned S-transforms at final station.

In order to illustrate the procedure presented in the previous section, I now proceed to compute the shifted S-Transform S_{2s} corresponding to the final station. I apply the same shifts to the voices of the transform S_{2t} because it is also needed to compute the Generalized Time Shift. In Figure 4 I plot the results of shifting the transforms S_2 and S_{2t} to show that indeed their peaks have the same location as the peaks of the S-transform of the first station S_1. No changes in the amplitudes are introduced, as the amplitude scales in Figure 4 show. Next, in Figure 5a, I plot the amplitude of the Cross-S-Transform $S_C(t, f_n)$ between the first and last stations. Even though all the information to obtain the dispersion curve is given by $S_C(t, f_n)$, it is not visually identifiable in Figure 5a, and a reassignment $S_C(t, f_n)$ might be convenient. In Fig. 5b I plot the normalized amplitude $\tilde{A}_{RC}(T_p, f)$ of the Reassigned Cross-S-Transform, which I compute in the following manner:

$$\tilde{A}_{RC}(T_p, f) = \frac{A_{RC}(T_p, f)}{\max\limits_{T_p, f} A_{RC}(T_p, f)} \tag{45}$$

where $A_{RC}(T_p, f)$ is the amplitude of $S_{RC}(T_p, f_n)$. The vertical axis of the RCST in Fig. 5b corresponds then to the time-shift. It can be observed that the concentration of energy of the RCST around the time shift is very high, to the point that the non-zero points of the RCST are not very visible in Fig. 5b. That is why in Figure 5c, where I compare the estimated slowness with the original slowness of Figure 1b (shown with the continuous line), I added black dots to make the non-zero points of the RCST more discernable. To obtain the dispersion curve of Fig. 5c, I simply divided the time shift axis of the RCST by the interstation distance, which in this case is 0.1 km.

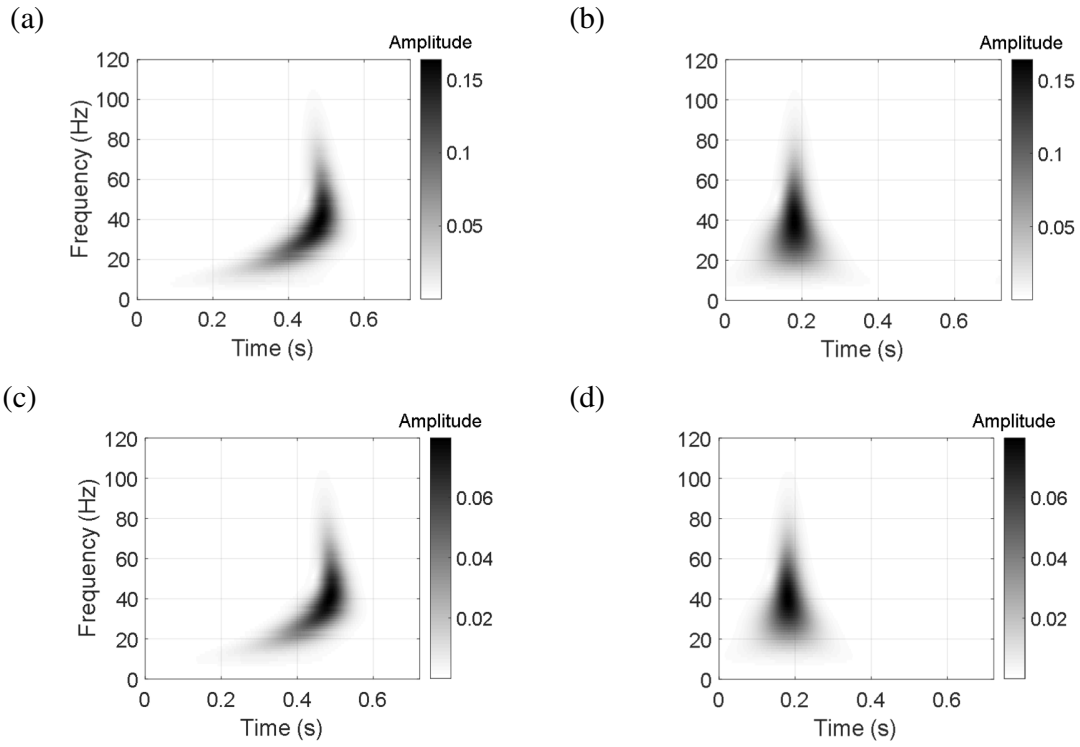

Figure 4. Amplitude of S-transforms of dispersed Ricker wavelet at last station. (a) Regular S-Transform, S_2, (b) Shifted S-Transform, S_{2s}, (c) S-Transform S_{2t}, (d) Shifted S-Transform S_{2st}.

295

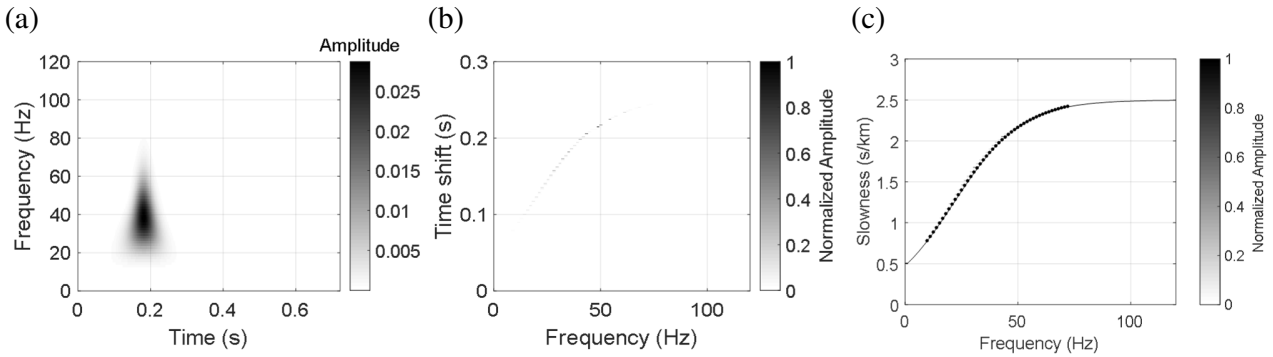

Figure 5. Single Ricker wavelet with artificial dispersion. (a) Amplitude of CST, (b) Amplitude of Reassigned CST (c) Dispersion curve compared with the original slowness curve (the continuous line).

Figure 5c illustrates that with the RCST very precise estimations of the slowness curve can be obtained. However, for signals composed of a non-contaminated single wave train, the computational cost of estimating the RCST is not justified, as simple Fourier analysis as in [20] provides very accurate results for the time shift. One advantage that the RCST over other methods of analysis is that its non-zero values are associated to the energy of the wave train present in the signal, and therefore, discerning the physical wave trains from noise or interfering waves becomes easier. As it can be observed in Figure 5c, the RCST gives values for slowness only within the frequency band of the wave train.

6. Example with two artificial dispersive wave trains propagating in the same direction

In this example I add another wave train to the signals, with a different artificial dispersion curve. In this way I intend to simulate the propagation of bi-modal dispersive waves. I add another Ricker to the first mode I already analysed, with a lower amplitude $A_{R2} = 0.5$, central frequency $f_{c2} = 60\ Hz$, and $t_{c2} = 1/f_{c2}$. For this new "higher mode" the slowness law is shown in Figure 6a with the thicker line, and the mathematical expression for the phase velocity is

$$V_{p2} = 4\exp\left(-\frac{f}{17}\right) + 0.55 \quad \left(\frac{km}{s}\right) \tag{46}$$

I adopt again 20 stations spaced at 5 m to propagate the wavelets, the resulting waveforms are shown in Figure 6b. From the signals of Figure 6b it is not evident if the two propagated modes are separated in time. However, from inspection of the S-transforms of the first and last stations, shown in Figures 7a and 7b, it is clear that the two modes are mixed at the first station, but separated at the final station. Thus, the strategy I follow here to compute the dispersion curve is different from the previous example. Instead of only using the first and last stations to compute the dispersion curve, I compute the dispersion curve between each pair of adjacent stations, and average the result after normalizing each dispersion curve according to Eq. (45). The final average dispersion curve is shown in Figure 7c, and compared with the original slowness curves. Even though the dispersion curve of second mode is less energetic, is correctly identified in the RCST. At about 50 Hz, the dispersion curve for the first mode moves away from the original slowness curve, and some spread of energy can be observed. This is indeed related to the mixture of the two modes, and one approach to improve the results would then be the analysis at stations farther from the source, where the two modes might be better separated. An alternative way to reduce this effect is to separate the two modes in the seismogram, before the dispersion analysis. However this solution requires measurements of at least two components (horizontal and vertical) of the waveforms at each station, usually unavailable in geophysical measurements, which retain only the vertical component. I will explore further this approach in the example of section 8.

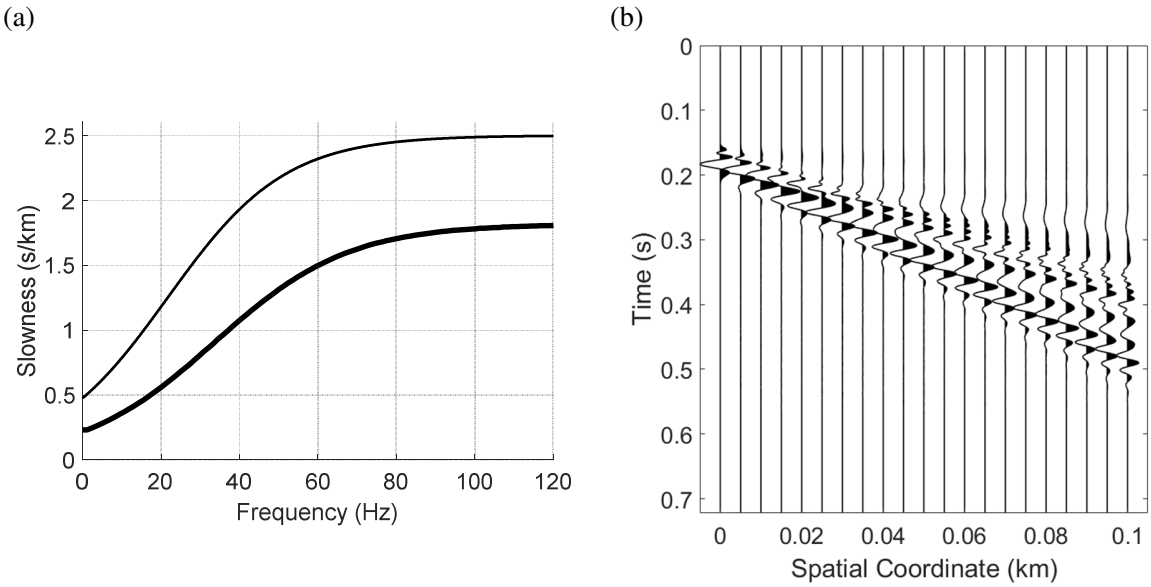

Figure 6. Artificial bi-modal dispersive Ricker wave train. (a) Slowness function, (b) Waveforms of propagated waves at 20 stations.

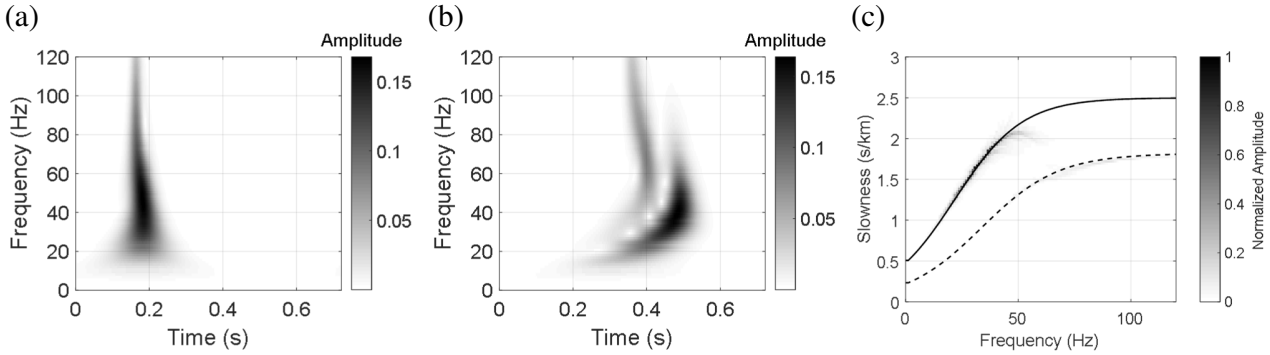

Figure 7. Bi-modal Ricker wavelet with artificial dispersion. (a) S-Transform at first station, (b) S-Transform at last station, (c) Average dispersion curve compared with the original slowness curve (the continuous line).

7. Example with two artificial dispersive wave trains propagating in opposite directions

In this experiment I consider the same two Ricker wave trains (modes) used in the previous example, but now the weaker wave train propagates in the opposite direction. With this experiment I try to simulate the presence of reflected/refracted waves in the signals, and investigate the effect on the estimated dispersion curve. The time histories of the waveforms are shown in Figure 8a, where it can be observed that the interference between the wave trains starts

at 0.06 km. In Figure 8b I present the average dispersion curve, which I obtained in the manner explained in the previous example. One effect that can be observed in Figure 8b is the "spreading" of the energy due to the interference between the wave trains. A weak presence with negative slope is also noticeable in Figure 8b, and how it diverts the dispersion curve after 50 Hz. In situations like this example, separation of the dispersive waves from the reflections/refractions can improve the accuracy of the slowness curve. However, the analyst should also keep in mind that the presence of those reflections/refractions might indicate lateral/horizontal heterogeneities in the velocity structure.

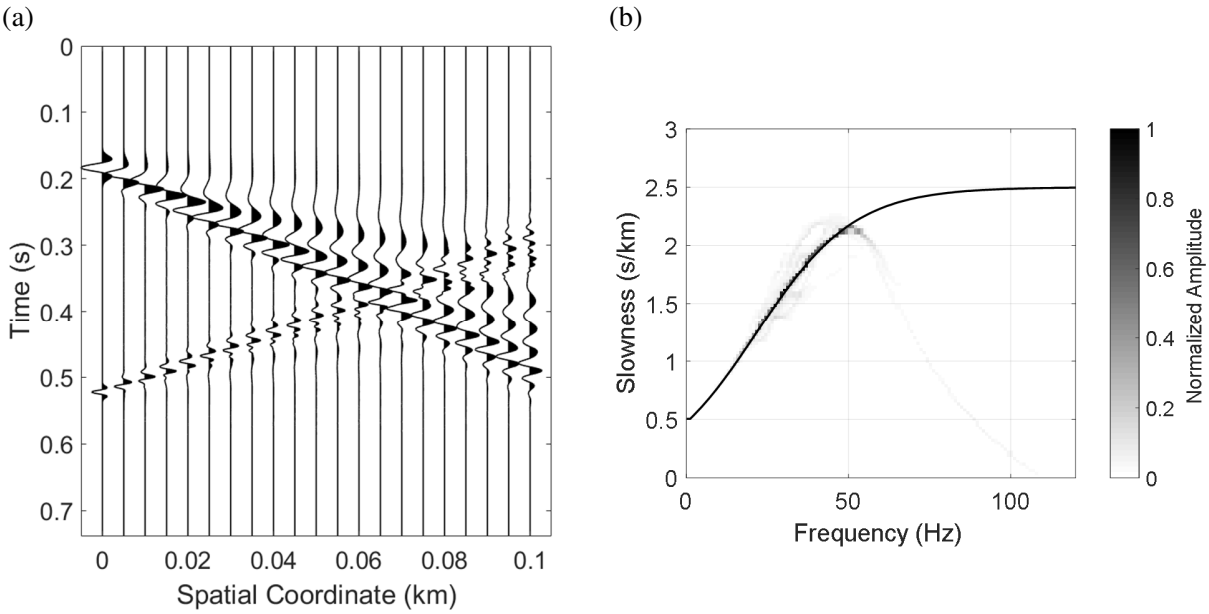

Figure 8. Artificial dispersive waves propagating in opposite directions. (a) Waveforms at 20 stations, (b) Average dispersion curve compared with the original slowness curve (the continuous line).

8. Example of mode separation from numerical simulations

In this last example I investigate the benefits of mode separation in the estimation of the dispersion curves. An efficient technique based on the S-Transform to identify and separate wave trains in seismograms has been proposed in the recent years [8], which provides the time histories of the extracted waves. However, the extraction technique is based on the polarization

characteristics of the waves and therefore it requires the vertical component and at least one horizontal component of the recorded/generated time histories, while most near-surface surveys retain only the vertical component. As it is the case in MASW surveys, the seismic source is a vertical force at the free surface of an earth model. In order to simulate a wave field with geometrical dispersion, the selected earth model is composed of several layers with different density and elastic constants. I adopt the earth model described in Table 1, which was already used by Xia *et al*. [16] in numerical simulations for parametric studies on inversion of velocity profiles from the fundamental mode of Rayleigh waves. With the mechanical parameters listed in Table 1 I then compute the Rayleigh wave theoretical dispersion curve with the software Gplivemodel [21], a Geopsy tool to compute dispersion curves for layered 1D earth models using the propagator-matrix method [23]. Figure 9 shows the resulting theoretical slowness curves for Rayleigh waves, and that around 15 Hz the curves of the fundamental and first higher mode are in close proximity.

Table 1. Mechanical parameters of layered earth model.

Layer	$v_s\ (m/s)$	$v_p\ (m/s)$	$\rho\ (g/cm^3)$	Thickness (m)
1	194	650	1.82	2.0
2	270	750	1.86	2.3
3	367	1400	1.91	2.5
4	485	1800	1.96	2.8
5	603	2150	2.02	3.2
Half-space	740	2800	2.09	

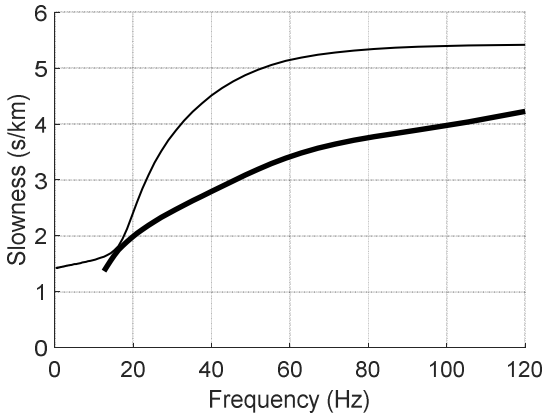

Figure 9. Theoretical slowness curves (fundamental and first higher mode) for Rayleigh waves in the earth model of Table 1. The thicker line corresponds to the higher mode.

365

366 To propagate Rayleigh waves I limit a rectangular region of the earth model to have 160 m of
367 length and 36 m of total depth, so that all layers described in Table 1 are considered. I then
368 discretize the 2D P-SV case of the wave equation for this region, using the Spectral Element
369 Method (SEM) [24]. The square elements have a size of 2x2 m, and the degree of the interpolant
370 of the field variables is 4. The top boundary of the 2D spatial region corresponds to the free
371 surface, whereas the other three boundaries have to comply with the condition of energy radiated
372 to the infinity, as illustrated in Figure 10a. To enforce such radiation condition I implement the
373 Multi-axial Perfectly Match Layer (M-PML) [25], an accurate and stable absorbing boundary for
374 isotropic elastic media. Each M-PML termination has 10 elements parallel to the truncated
375 boundary. The discretization in time of the equation of motion is made with the midpoint rule
376 with a time step Δt=4.93E-05 s. I use again a Ricker wavelet with a central frequency of 20 Hz
377 to describe the time-variation of the source. The source, imposing a vertical force at the surface,
378 is located at 10 m from the first receiver. The interstation distance for the receivers is 2 m. The
379 resulting time histories of the vertical and horizontal displacement at 41 receivers on the free

surface are shown in Figure 10b and 10c, respectively. The propagation of the two first modes of Rayleigh waves is clearly distinguished along the stations.

I select the vertical component of the waveforms to estimate the dispersion curve, usually preferred to avoid the presence of other dispersive waves (such as Love waves) in the signal. In this 2D P-SV simulation Love waves cannot be generated, nevertheless I make the initial analysis with the vertical component. The resulting slowness curve is shown in Figure 11a, where I again added some black dots on the non-zero values of the RCST to improve the clarity of the plot. Even though the simulations seem to be of high accuracy as there is no contamination due to reflections from the absorbing boundaries, several problems are observed with dispersion curve of Figure 11a. First, the higher mode is barely detected, because of the small energy compared to the fundamental mode. And second, at around 15 Hz the higher mode is misidentified as the continuation of the fundamental mode. In Figure 11b I add the theoretical curves to compare with the obtained results, where the misidentification problem is more evident. In real cases, where there are no "theoretical curves" available to the analyst, the mode misidentification problem can be overlooked, leading to incorrect inverted velocity profiles.

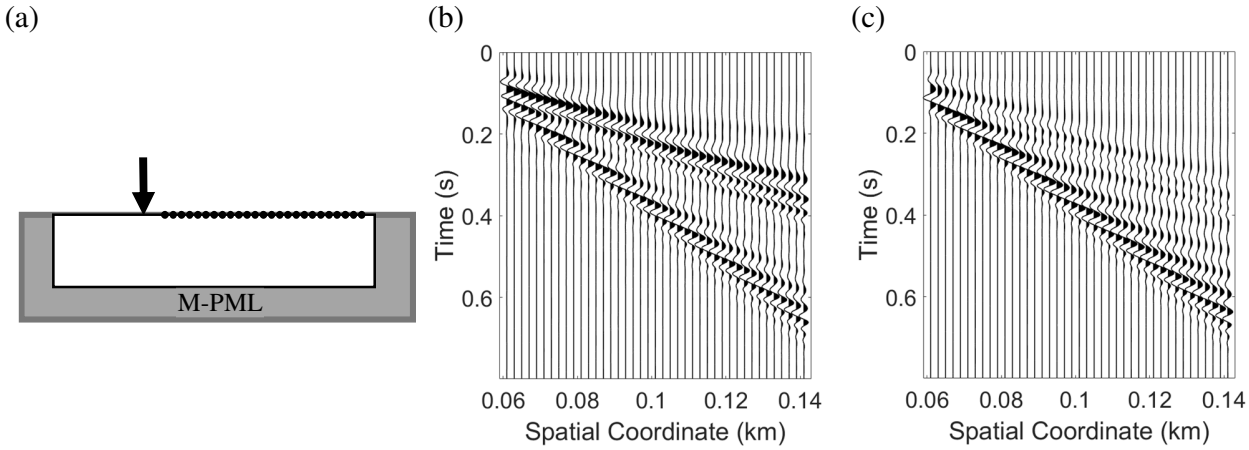

Figure 10. 2D Numerical simulation of seismic wave propagation in a layered medium. (a) Sketch of the propagating medium, with location of the source, receivers and absorbing boundaries. (b) Time histories of horizontal displacements, (c) Time histories of vertical displacements.

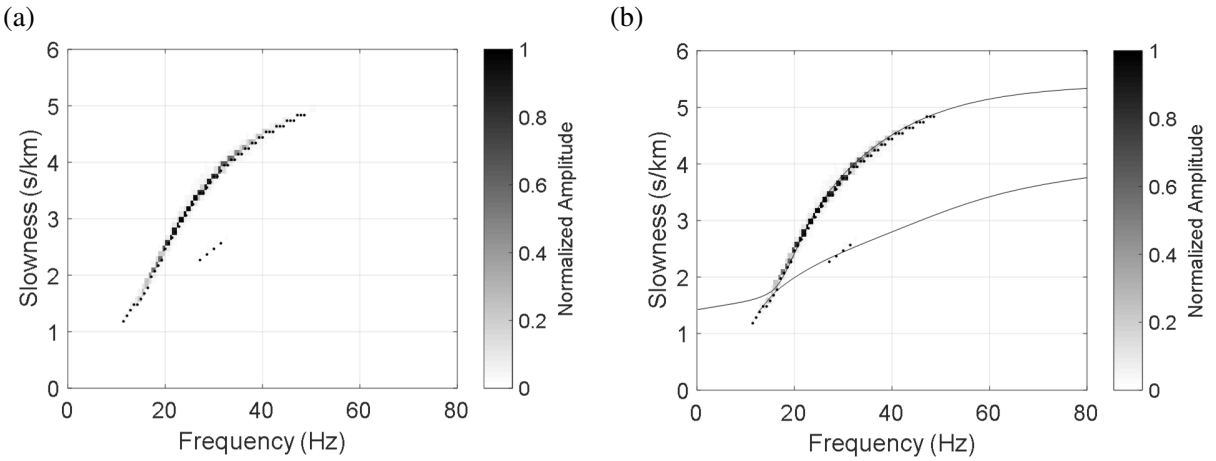

Figure 11. Average slowness curves from vertical component of simulated Rayleigh waves. (a) Dispersion curve from RCST, (b) Dispersion curve from RCST compared with theoretical curves.

The strategy I propose here to avoid the misidentification problem is to separate the two Rayleigh modes present in the signals with the *Normalized Inner Product* (NIP). For details on the application of the NIP technique to multi-component recordings, the reader is referred to the references [8], [9]. Because the NIP is a time-frequency technique that identifies and extract the waves according to their polarization characteristics, it efficiently identifies Rayleigh waves, which are elliptically polarized waves. In most cases the fundamental mode of Rayleigh waves has a *retrograde motion* at shallow depths, meaning that the particle motion is an elliptical rotation against the propagation direction. In other cases the fundamental mode and/or the higher modes can present *prograde motion* at the surface, an elliptical rotation in the same direction of wave propagation.

In Figure 12a I plot the vertical component of the time histories of the retrograde waves extracted with the NIP, and it is clear that they correspond to the fundamental mode. Fortunately, when extracting the prograde waves, also with the NIP, I found that they correspond to the less energetic higher mode of the Rayleigh waves, as shown in Figure 12b; and then the two modes

411 have been successfully separated. The time histories of the separated waves are then used to
412 compute the slowness curves shown in Figure 13, where the comparison with the theoretical
413 curves is included. It is evident that after mode separation, the estimated dispersion curves are
414 very precise, and the mode misidentification problem is resolved.

415

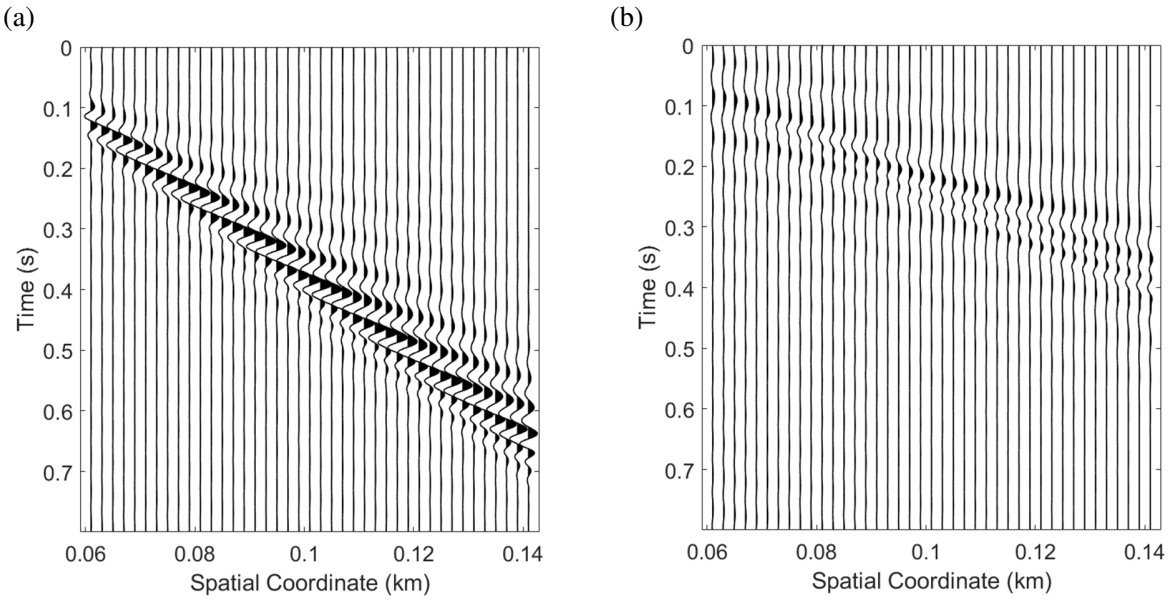

Figure 12. Vertical component of time histories of simulated Rayleigh waves. (a) Fundamental mode (retrograde motion), (b) First higher mode (prograde motion).

416

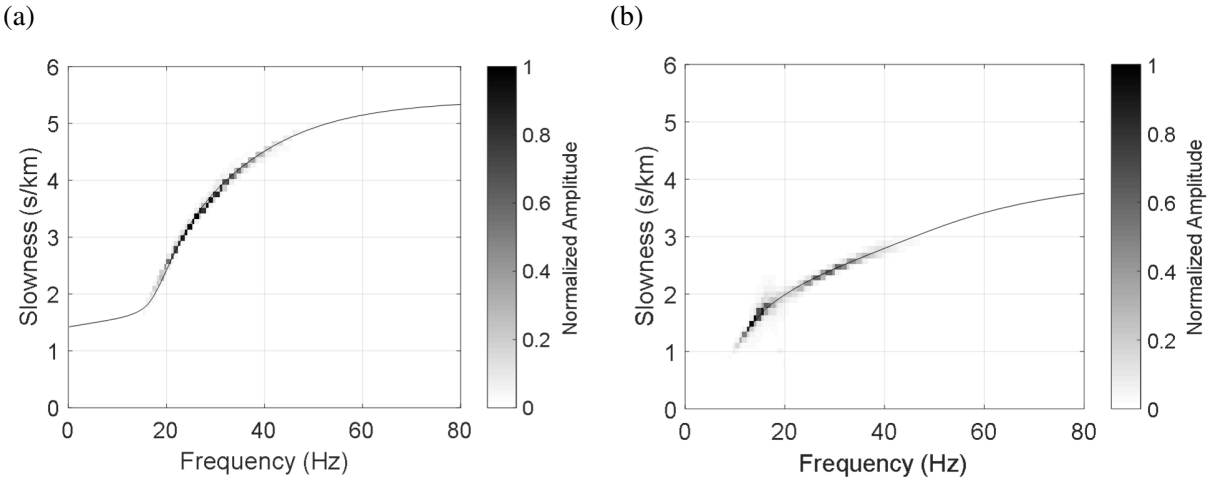

Figure 13. Average slowness curves from vertical component of simulated Rayleigh waves. (a) Fundamental mode, (b) First higher mode.

417 **9. Example with real recordings**

418 In this example, I estimate the dispersion curve via the RCST from actual recorded data which is
419 provided with the software Geopsy [21], an open source tool for geophysical research and
420 applications (*e.g.*, [22]). The 1D linear arrangement of seismic surface wave recordings is to be
421 analyzed with the active seismic experiment (MASW) tool implemented in Geopsy, based on the

F-K transform. The profile of recorded waveforms is presented in Figure 14, where for clarity I normalized each time history by its maximum amplitude. The active source is located at 4 m from the first sensor, and the interstation distance of the 24 sensors is also 4 m. The time step of the time histories Δt =2.5E-4. Figure 14 clearly shows that there are at least two modes propagating through the different stations, as well as other wave types interfering with the modes.

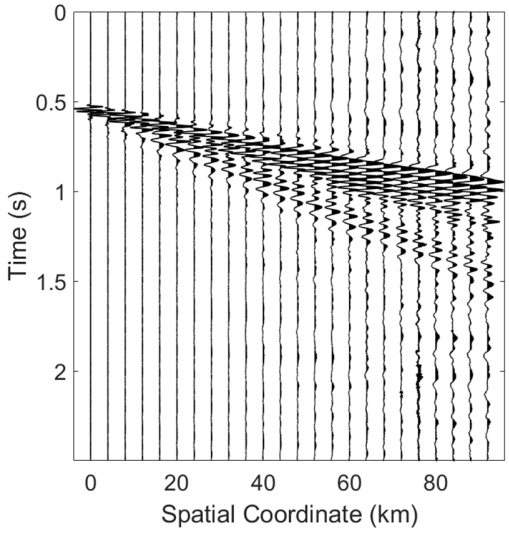

Figure 14. Recorded waveforms at 24 stations in a MASW survey.

In Figure 15 I compare the slowness curves obtained with the RCST with the results given by the active MASW tool of Geopsy. For clarity, I added the black dots to the peaks of the RCST. The figures illustrate that the two methods give similar results, and they both identify well the higher mode, whereas the fundamental mode is well defined up to 20 Hz. The RCST gives shaper results in more limited frequency bands, because the RCST gives non-zero values only at frequencies with relatively high concentration of energy. Furthermore, considering the analysis of the previous artificial examples, the RCST of Figure 15a indicates that the fundamental mode is interfered not only by the higher mode and noise, but also by some reflected/refracted waves. This observation needs to be taken into consideration if the dispersion curve will be used to

invert a velocity profile, whether those interfering waves are related to the physical process or not.

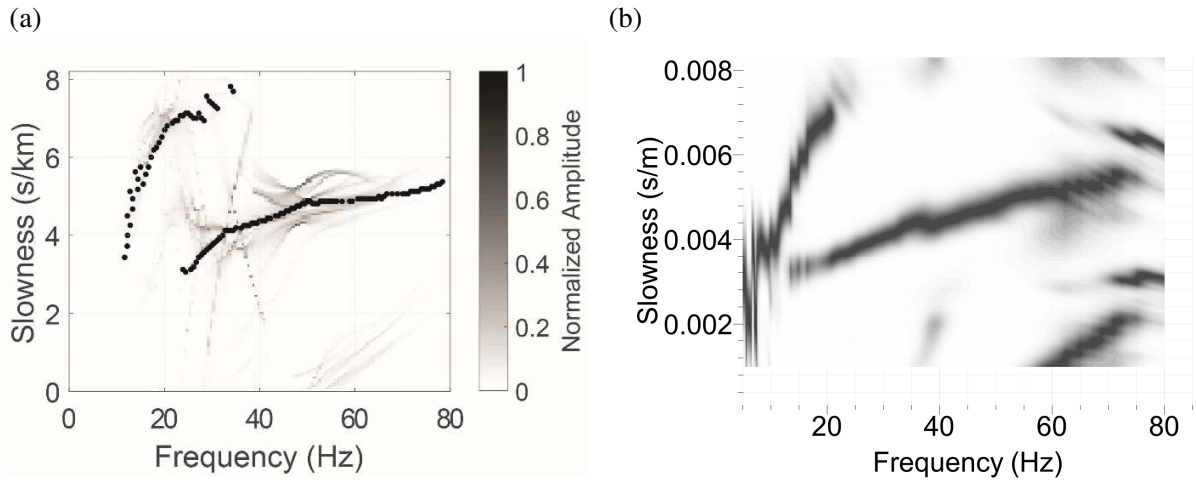

Figure 15. Slowness curves of recorded waveforms. (a) Average dispersion curve from RCST, (b) Dispersion curve from Geopsy software.

10. Conclusions

In this work, I proposed a technique to estimate dispersion, slowness curves for multimodal, non-stationary signals, based on the Reassigned Cross-S-Transform. I presented in detail the mathematical derivations and the computational steps for the construction of the RCST. The RCST I proposed is derived from simple maximization principles so that the energy is concentrated at the ridges of the time-frequency representations of the signals. Furthermore, in deriving the RCST I made no assumptions regarding the types of waves or the cinematics of the physical process. The objective of the proposed reassignment is twofold (i) improve the resolution of the time-frequency representation, and (ii) concentrate the energy of two signals in the neighborhood of the time-shift related to directly provide the phase velocity. An additional advantage of the procedure I propose is that because the time shift between signals is obtained from cross-correlation, no time readings are needed, and dispersion curves can be computed for data that is not synchronized with the same initial time. I illustrated the application of the RCST

with seismic signals containing dispersive waves, constructed from artificial dispersion curves, generated via 2D numerical simulation, and recorded in a real survey. The examples with multi-modal artificial waves allowed to recognize the effects on the dispersion curve of modes overlapping in time and frequency, and the effects of possible reflections/refractions present in the signals. Regardless of the identified detrimental effects, the dispersion curves of the different artificial modes were well identified with the RCST. The analysis is then helpful to interpret the dispersion curves from real seismic recordings containing multi-modal Rayleigh waves, for which the RCST provides very sharp dispersion curves. Furthermore, I showed that combining the RCST with the NIP technique of extraction of dispersive waves is an effective strategy to the correct identification of modes, in particular when the dispersion curves are in close proximity.

11. Acknowledgements

The author would like to thank Prof. Apostolos Papageorgiou for discussions on the reassignment technique, and two anonymous reviewers for constructive comments that improved the manuscript. This research has been financed by the French National Research Agency (Agence National de la Recherche), under project MODULATE, grant number ANR-18-CE22-0017.

12. References

[1] R. N. Bracewell, “The Fourier Transform and applications,” *McGraw Hill*, pp. 1–10, 2000.

[2] S. Mallat, *A Wavelet Tour of Signal Processing, Third Edition: The Sparse Way*, Third edit. Academic Press, 2008.

[3] A. Grossmann and J. Morlet, “Decomposition of hardy functions into square integrable

wavelets of constant shape," *SIAM J. Math. Anal*, vol. 15, no. 4, pp. 723–736, 1984.

[4] R. G. Stockwell, L. Mansinha, and R. P. Lowe, "Localization of the Complex Spectrum: The S Transform," *IEEE Trans. Signal Process.*, vol. 44, no. 4, pp. 998–1001, 1996.

[5] N. E. Huang *et al.*, "The empirical mode decomposition and the Hilbert spectrum for nonlinear and non-stationary time series analysis," *Proc. R. Soc. Lond., Ser. A, Math. Phys. Eng. Sci*, vol. 454, pp. 903–995, 1998.

[6] S. Meignen, T. Oberlin, and D. H. Pham, "Synchrosqueezing transforms: From low- to high-frequency modulations and perspectives," *Comptes Rendus Phys.*, vol. 20, no. 5, pp. 449–460, 2019.

[7] K. Kodera, R. Gendrin, and C. Villedary, "Analysis of time-varying signals with small bt values," *IEEE Trans. Acoust. Speech Signal Process*, vol. 26, pp. 64–76, 1978.

[8] K. C. Meza-Fajardo, A. S. Papageorgiou, and J. F. Semblat, "Identification and extraction of surface waves from three-component seismograms based on the normalized inner product," *Bull. Seismol. Soc. Am.*, vol. 105, no. 1, pp. 210–229, 2015.

[9] K. C. Meza-Fajardo and A. S. Papageorgiou, "Estimation of rocking and torsion associated with surface waves extracted from recorded motions," *Soil Dyn. Earthq. Eng.*, vol. 80, 2016.

[10] R. Stockwell, "Why use the S-transform," in *seudo-Differential Operators: PDEs and Time-Frequency Analysis*, 2007, pp. 279–309.

[11] Y. Liu, W. Zhou, P. Li, S. Yang, and Y. Tian, "An Ultrahigh Frequency Partial Discharge Signal De-Noising Method Based on a Generalized S-Transform and Module Time-Frequency Matrix," *Sensors*, vol. 16, p. 941, 2016.

[12] Z. Huang, J. Zhang, and T. Zhao, “Synchrosqueezing based-transform and Its Application in Seismic Spectral Decomposition.,” *IEEE Trans. Geosci. Remote Sens*, vol. 54, pp. 817–825, 2015.

[13] G. Pan, S. Li, and Y. Zhu, “A time-frequency correlation analysis method of time series decomposition derived from synchrosqueezed S transform,” *Appl. Sci.*, vol. 9, no. 4, 2019.

[14] R. Askari, R. J. Ferguson, and K. DeMeersman, “Estimation of phase and group velocities for multi-modal ground roll using the ‘phase shift’ and ‘slant stack generalized S transform based’ methods,” 2011.

[15] A. Levshin and G. Panza, “Caveats in multi-modal inversion of seismic surface wavefields,” *Pure Appl Geophys*, vol. 163, pp. 1215–33, 2006.

[16] J. Xia, R. Miller, and C. Park, “Estimation of near-surface shear-wave velocity by inversion of Rayleigh waves,” *Geophysics*, vol. 64, no. 3, pp. 691–700, 1999.

[17] C. B. Park, R. D. Miller, and J. Xia, “Summary report on surface-wave project at Kansas Geological Survey,” Lawrence, Kansas, 1997.

[18] C. Park, R. Miller, and J. Xia, “Multichannel analysis of surface waves,” *Geophysics*, vol. 64, no. 3, pp. 800–8, 1999.

[19] K. Aki and P. Richards, *Quantitative Seismology*, Second edi. University Science Books, 2002.

[20] W. Sachse and Y. Pao, “On the determination of phase and group velocities of dispersive waves in solids,” *J. Appl. Phys.*, vol. 49, p. 4320, 1978.

[21] Geopsy-team, “Geopsy Project,” 2005. [Online]. Available: http://www.geopsy.org/index.html (Last accesed April-2020).

518 [22] M. Wathelet, B. Guillier, P. Roux, C. Cornou, and M. Ohrnberger, “Rayleigh wave three-
519 component beamforming: signed ellipticity assessment from high-resolution frequency-
520 wavenumber processing of ambient vibration arrays,” *Geophys. J. Int.*, vol. 215, no. 1, pp.
521 507–523, 2018.

522 [23] F. Gilbert and G. Backus, “Propagator matrices in elasticwave and vibration problems,”
523 *Geophysics*, vol. 31, pp. 326–332, 1966.

524 [24] K. C. Meza Fajardo and A. S. Papageorgiou, “Wave propagation in unbounded elastic
525 domains using the spectral element method: Formulation,” *Earthq. Struct.*, vol. 3, no. 3–4,
526 pp. 383–411, 2012.

527 [25] K. C. Meza-Fajardo and A. S. Papageorgiou, “A nonconvolutional, split-field, perfectly
528 matched layer for wave propagation in isotropic and anisotropic elastic media: Stability
529 analysis,” *Bull. Seismol. Soc. Am.*, vol. 98, no. 4, 2008.

530

List of figures captions

Figure 1. Artificial (a) phase velocity and (b) slowness for single dispersive Ricker wave train.

Figure 2. Waveforms at 20 stations for a single Ricker wavelet with artificial dispersion.

Figure 3. Amplitude of S-transforms of dispersed Ricker wavelet. (a) S-transforms at first station, (b) S-transforms at final station, (c) Reassigned S-transforms at first station (d) Reassigned S-transforms at final station.

Figure 4. Amplitude of S-transforms of dispersed Ricker wavelet at last station. (a) Regular S-Transform, $S2$, (b) Shifted S-Transform, $S2s$, (c) S-Transform $S2t$, (d) Shifted S-Transform $S2st$.

Figure 5. Single Ricker wavelet with artificial dispersion. (a) Amplitude of CST, (b) Amplitude of Reassigned CST (c) Dispersion curve compared with the original slowness curve (the continuous line).

Figure 6. Artificial bi-modal dispersive Ricker wave train. (a) Slowness function, (b) Waveforms of propagated waves at 20 stations.

Figure 7. Bi-modal Ricker wavelet with artificial dispersion. (a) S-Transform at first station, (b) S-Transform at last station, (c) Average dispersion curve compared with the original slowness curve (the continuous line).

Figure 8. Artificial dispersive waves propagating in opposite directions. (a) Waveforms at 20 stations, (b) Average dispersion curve compared with the original slowness curve (the continuous line).

Figure 9. Theoretical slowness curves (fundamental and first higher mode) for Rayleigh waves in the earth model of Table 1. The thicker line corresponds to the higher mode.

553 Figure 10. 2D Numerical simulation of seismic wave propagation in a layered medium. (a)
554 Sketch of the propagating medium, with location of the source, receivers and absorbing
555 boundaries. (b) Time histories of horizontal displacements, (c) Time histories of vertical
556 displacements.
557 Figure 11. Average slowness curves from vertical component of simulated Rayleigh waves. (a)
558 Dispersion curve from RCST, (b) Dispersion curve from RCST compared with theoretical
559 curves.
560 Figure 12. Vertical component of time histories of simulated Rayleigh waves. (a) Fundamental
561 mode (retrograde motion), (b) First higher mode (prograde motion).
562 Figure 13. Average slowness curves from vertical component of simulated Rayleigh waves. (a)
563 Fundamental mode, (b) First higher mode.
564 Figure 14. Recorded waveforms at 24 stations in a MASW survey.
565 Figure 15. Slowness curves of recorded waveforms. (a) Average dispersion curve from RCST,
566 (b) Dispersion curve from Geopsy software.
567